Supplementary Information

Binding kinetics of ultrasmall gold nanoparticles with proteins

André L. Lira[1], Rodrigo S. Ferreira[1], Ricardo J.S. Torquato[1], Huaying Zhao[2], Maria Luiza V. Oliva[1], Sergio A. Hassan[3], Peter Schuck[2], Alioscka A. Sousa*[,1]

1. Department of Biochemistry, Federal University of São Paulo, São Paulo, SP, Brazil

2. National Institute of Biomedical Imaging and Bioengineering, National Institutes of Health, Bethesda, MD, USA

3. Center for Molecular Modeling, OIR/CIT, National Institutes of Health, Bethesda, MD, USA

* Corresponding author: alioscka.sousa@unifesp.br

S1. Fluorescence titration quenching in the analysis of NP-CrataBL interactions

Steady-state fluorescence quenching offers a convenient means to probe the interactions of proteins with ultrasmall gold NPs. Typically, it is assumed that n proteins, P, can bind around the surface of a single nanoparticle, NP, according to:

$$nP + NP \rightleftarrows P_n \cdot NP$$

Fluorescence titration quenching is ordinarily performed utilizing a reverse titration scheme. Namely, a solution with fixed amount of protein (ligand), having an initial fluorescence signal F_0, is titrated with NPs (receptors). The observed extinction of protein fluorescence upon NP binding is then recorded as a function of NP concentration. The quenching efficiency is hardly expected to be 100%, thus the fluorescence signal at saturation, F_s, is typically a number larger than zero.

NP-CrataBL interactions, however, do not follow a simple equilibrium reaction as shown above. This is because CrataBL contains two or more surface patches where NPs can bind. This multivalent binding leads to crosslinking of NPs and the formation of NP/protein aggregates in PBS. The aggregates are not visible by eye under agitation, but can be detected by UV-vis spectroscopy (Fig. S4b). As a result of this multivalent binding, the fluorescence quenching methodology cannot be used for a true quantification of interactions [s1]. Additional challenges in quantification are discussed below and in ref.

[s2]. Nevertheless, fluorescence titration quenching can be used for a qualitative assessment of binding strength among different NPs, as a function of solution ionic strength, and in macromolecular crowded solutions, as discussed below and in the main text.

S2. Evaluation of picomolar binding affinity between AuMBA and CrataBL

We checked whether the pM binding affinity exhibited between AuMBA and CrataBL (site #1 from Table 1) could be corroborated by a set of additional experiments, as described next.

i) Fluorescence titration quenching

Analysis of the fluorescence data obtained at 150 mM NaCl (Fig. 2 in the main text) does not support either the presence or lack of a pM binding site on CrataBL. To better illustrate this point, we simulated fluorescence quenching data assuming that each protein was able to accommodate two NPs simultaneously. In the simulations, it was assumed that the NPs bind CrataBL with both a high and intermediate K_D of 0.1 nM and 100 nM – corresponding to the range of K_{Ds} for sites #1 and #2 as assessed by SPR (Table 1). As shown in Fig. S8a, the NPs saturate the high-affinity site on the protein before the second site is occupied. It is reasonable to assume that the first binding event quenches most but not all of the protein fluorescence (e.g., 80% quenching). It is seen that the second binding event creates a curvature in the quenching curve starting at the level of the remaining protein fluorescence (at 20% quenching). Fitting the data to a quadratic equation [s2] yields a K_D of 60 nM, i.e., the high-affinity site remains "invisible".

Nevertheless, by taking the set of titration curves as a function of NaCl concentration as a whole (Fig. 2), it is possible to infer that AuMBA does not bind CrataBL with pM affinity at 150 mM. Fig. S8b shows simulated NP-protein quenching data for different values of the affinity constant K_D, and assuming $F_0 = 1$, $n = 1$, $F_s = 0$ and $[P]_t = 1$ μM. When the K_D falls below ~ 10 nM, the traces become indistinguishable from each other – the stoichiometric binding condition ($K_D << [P]_t$). Regarding AuMBA-CrataBL in Fig. 2, it can be seen that the quenching curves become progressively steeper as the salt concentration is reduced from 500 to 50 mM, while a further decrease in salt concentration down to 10 mM does not bring significant changes to the quenching profile. This behavior might be taken to suggest that K_D is at least in the low nM range at 50 mM (the stoichiometric binding condition), but higher at 150 mM.

(ii) Estimation of k_{off}

Table 1 reveals that the pM binding affinity was mostly the result of a dissociation rate constant on the order of 10^{-4} s^{-1}. Such small k_{off} would entail the formation of a very stable, long-lived AuMBA-CrataBL complex with a $t_{1/2}$ of 115 min. We therefore implemented a dissociation assay to get a rough estimation of the value of k_{off}. As shown in Fig. 9, comparison with simulations clearly ruled out the possibility of a k_{off} in the range of 10^{-4} s^{-1}. The experimental results were consistent with a k_{off} roughly around $0.5x10^{-2}$ s^{-1}, which matches approximately the k_{off} for site #2 in Table 1.

(iii) Isothermal titration calorimetry (ITC)

In favorable cases, ITC can directly resolve the presence of two binding sites with high and intermediate affinities on a protein surface. In order to detect the individual binding events from a single titration series, two conditions must be met: (i) the ITC signals (heats) must be of sufficiently different magnitude and (ii) negative binding cooperativity (arising from the binding of several proteins to a single NP) must be absent. This can be best illustrated with simulations (Fig. S10a). Experimental ITC data was recorded on the AuMBA-CrataBL system at 150 mM NaCl by titrating AuMBA with CrataBL. This yielded a reasonably well-behaved ITC isotherm, from which a single K_D of 230 nM was calculated (Fig. S10b). Although this result must be interpreted with caution due to the underlying constraints (i,ii) as noted above, at first sight it supports the contention that AuMBA does not bind CrataBL in the pM range of affinities. The K_D of $\sim$ 230 nM found by ITC compares well with the K_D of 35 nM for site #2 in Table 1 (a 6.5-fold difference).

(iv) Conclusions

Given the collective evidence, the above results indicate that site #1 (Table 1) is an artifact of the SPR assay. One possible explanation for the pM binding affinity of site #1 would be the occurrence of AuMBA rebinding during the dissociation phase, which would lead to an artifactual decrease in the value of k_{off}. Rebinding is a manifestation of mass-transport limitations when the association rate constant is fast (> 10^6 $M^{-1}s^{-1}$), i.e., the NPs rebind the surface before they have time to diffuse away from it. The impact of mass transport limitation scales with the total number of surface sites, therefore the observed similarity of distributions obtained at different immobilization levels suggests this not to be the cause (Fig. S6). More likely, the artifactual pM affinity is the result of avidity effects, which would reduce k_{off} significantly while causing no major changes to k_{on}. In principle, it might appear that such explanation should be ruled out given the consistent

results obtained for the different CrataBL surfaces. However, there is little evidence that immobilization is spatially uniform across the SPR surface; rather, it seems more likely that lateral or perpendicular immobilization zones of varying extent exist [s3-s4]. Furthermore, it is possible that CrataBL has a tendency to be immobilized in clusters. In either of these cases avidity effects might still ensue under lower total protein surface coverages.

It should be possible to test for the occurrence of avidity and/or rebinding effects in SPR with suitable control experiments, including: a co-injection of CrataBL and AuMBA in the flow to evaluate whether the soluble protein can compete with immobilized CrataBL for binding to AuMBA; addition of CrataBL in the dissociation buffer to evaluate whether the soluble protein can prevent the dissociating AuMBA from rebinding to the surface; a change in the experimental setup by immobilizing AuMBA and injecting CrataBL in the flow instead. Unfortunately, none of these possibilities proved fruitful in practice because of high levels of nonspecific CrataBL binding to the dextran matrix. Incidentally, this nonspecific binding of CrataBL to dextran is a clue that immobilization will likely not be uniform, but rather go to the first sites it sees, which are on fronts of immobilization.

References

s1. Bujalowski, W. & Jezewska, M.J. Quantitative thermodynamic analyses of spectroscopic titration curves. *Journal of molecular structure* **1077**, 40-50 (2014).

s2. Sousa, A.A. A Note on the use of Steady-State Fluorescence Quenching to Quantify Nanoparticle-Protein Interactions. *J. Fluoresc.* **25**, 1567-1575 (2015).

s3. Zacher, T. & Wischerhoff, E. Real-time two-wavelength surface plasmon resonance as a tool for the vertical resolution of binding processes in biosensing hydrogels. *Langmuir* **18**, 1748-1759 (2002).

s4. Schuck, P. & Zhao, H. The role of mass transport limitation and surface heterogeneity in the biophysical characterization of macromolecular binding processes by SPR biosensing. *Surface plasmon resonance: methods and protocols*, 15-54 (2010).

s5. Zhang, F., Walcott, B., Zhou, D., et al. Structural studies on the interaction of Crataeva tapia bark protein with heparin and other glycosaminoglycans. *Biochemistry* **52**, 6275-6285 (2013).

s6. Alsallaq, R. & Zhou, H.X. Electrostatic rate enhancement and transient complex of protein–protein association. *Proteins: Structure, Function, and Bioinformatics* **71**, 320-335 (2008).

s7. Suh, J., Tang, C. & Clore, G. M. Role of electrostatic interactions in transient encounter complexes in protein-protein association investigated by paramagnetic relaxation enhancement. *J. Am. Chem. Soc.* **129**, 12954-12955 (2007).

s8. Schreiber, G. & Fersht, A.R. Rapid, electrostatically assisted association of proteins. *Nature Structural & Molecular Biology* **3**, 427-431 (1996).

Table S1. Individual affinity and kinetic constants for AuMBA-CrataBL interactions. Values determined by integration of the major peaks in the surface-site distribution plots of Fig. S6.

CrataBL	320 RU			1280 RU			2200 RU		
Site	1	2	3	1	2	3	1	2	3
K_D(M)	9.7×10^{-11}	3.9×10^{-8}	1.1×10^{-6}	7.4×10^{-11}	2.5×10^{-8}	2.2×10^{-6}	5.4×10^{-11}	4.2×10^{-8}	1.5×10^{-6}
k_{on} ($M^{-1}s^{-1}$)	3.7×10^{6}	2.7×10^{5}	2.9×10^{5}	0.73×10^{6}	5.3×10^{5}	0.77×10^{5}	0.70×10^{6}	0.87×10^{5}	1.4×10^{5}
k_{off} (s^{-1})	3.6×10^{-4}	1.1×10^{-2}	3.1×10^{-1}	0.54×10^{-4}	1.3×10^{-2}	1.7×10^{-1}	0.38×10^{-4}	0.37×10^{-2}	2.2×10^{-1}

Table S2. Individual affinity and kinetic constants for AuGSH-CrataBL interactions. Values determined by integration of the major peaks in the surface-site distribution plots of Fig. S7.

CrataBL	950 RU	2090 RU
K_D(M)	1.5×10^{-5}	1.5×10^{-5}
k_{on} ($M^{-1}s^{-1}$)	1.5×10^{4}	2.2×10^{4}
k_{off} (s^{-1})	2.2×10^{-1}	3.2×10^{-1}

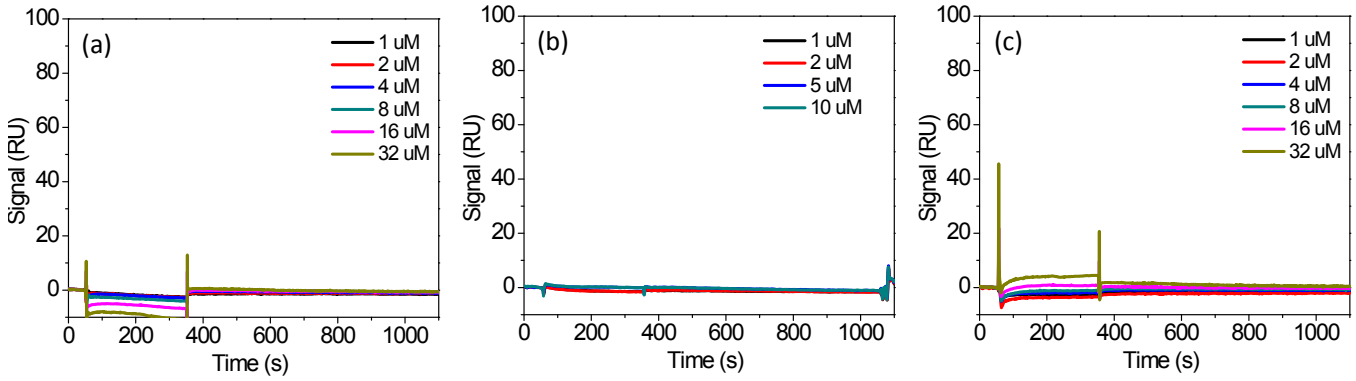

Figure S1. SPR measurements of AuGSH interactions with trypsin, chymotrypsin and lysozyme. No interactions were observed between AuGSH and immobilized (**a**) trypsin, (**b**) chymotrypsin and (**c**) lysozyme. Proteins were immobilized in a CM5 chip at 1000 RU. AuGSH concentrations: 1, 2, 4, 8, 16, 32 μM for trypsin and lysozyme; 1, 2, 5, 10 μM for chymotrypsin. Flow rate, 30 μL/min.

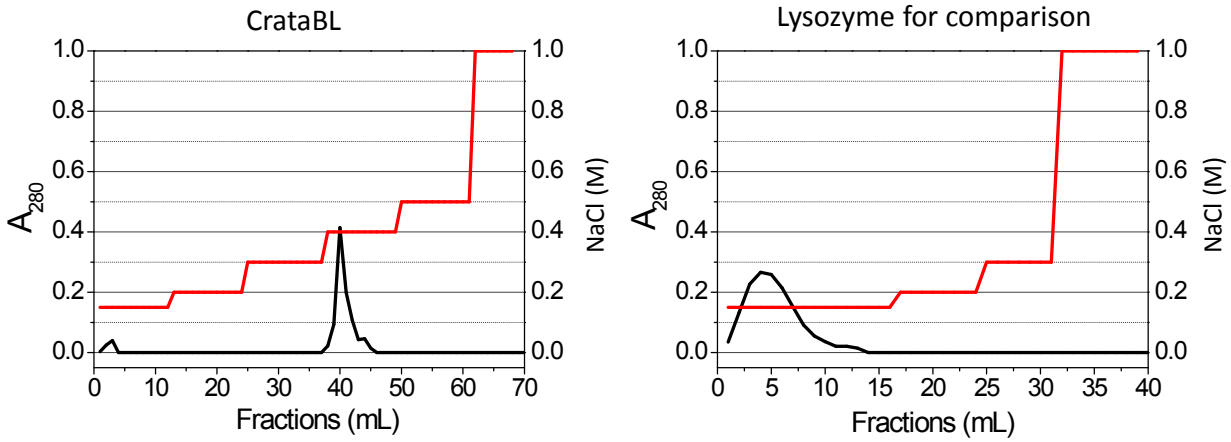

Figure S2. CrataBL as a heparin-binding protein [s5]. CrataBL (21 kDa, pI = 10.5) was loaded into a heparin column that had been pre-equilibrated with phosphate buffer (pH 7.4) without NaCl. Elution of CrataBL was accomplished using an NaCl concentration gradient. The protein does not elute from the column until the salt concentration has reached 0.4 M. The same procedure was repeated with lysozyme. In contrast to CrataBL, lysozyme (14.3 kDa, pI = 11.3) elutes at much lower salt concentration (0.15 M) despite also being a small and highly basic protein.

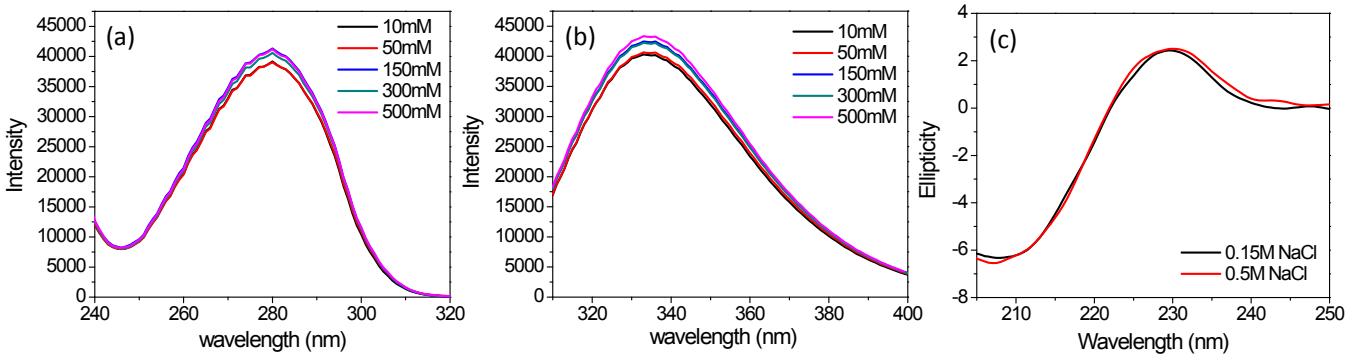

Figure S3. Excitation, emission and circular dichroism (CD) spectra of CrataBL recorded under different NaCl concentrations. a, Excitation spectra. Recorded with Em = 340 nm. **b,** Emission spectra. Recorded with Ex = 280 nm. Slit widths = 5 nm. **c,** CD spectra. [CrataBL] = 2 μM (a,b) and 10 μM (c). T = 20 °C.

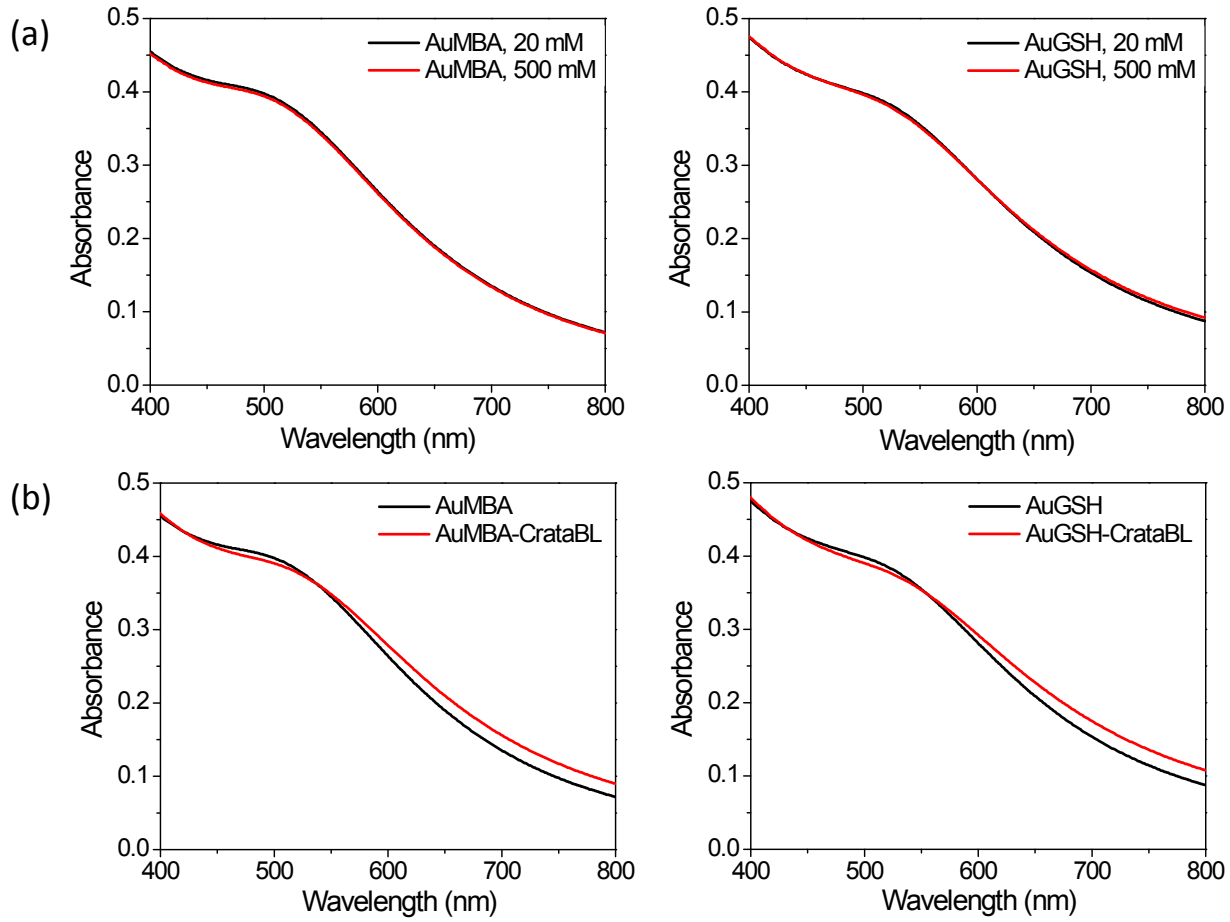

Figure S4. UV-vis spectra of NPs and NP/CrataBL complexes. a, Spectra of NPs showing lack of aggregation at up to 500 mM NaCl. **b,** Spectra of NP-CrataBL complexes suggesting some NP aggregation in the presence of CrataBL at 150 mM NaCl. The incubation time was 4 hours.

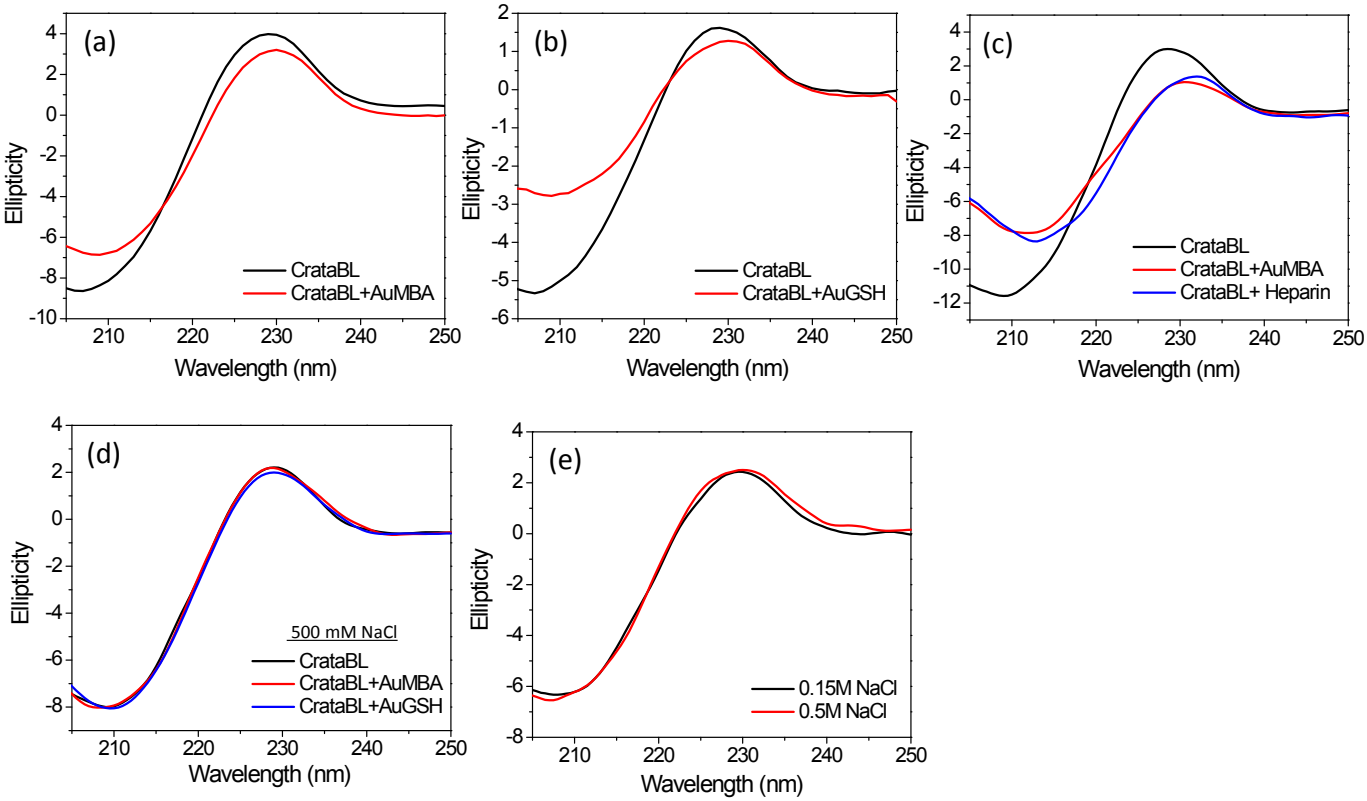

Figure S5. Circular dichroism spectra of CrataBL. a, Secondary structure of CrataBL is altered upon interactions with AuMBA at 150 mM NaCl. CrataBL, 10 μM; AuMBA, 2 μM; **b,** Same for AuGSH. CrataBL, 5 μM; AuGSH, 4 μM; **c,** Binding of heparin to CrataBL causes similar changes in secondary structure relative to binding of NPs. CrataBL, 10 μM; heparin, 20 μM. **d,** Changes in secondary structure (as seen in a,b) are reversed when interactions are screened at higher ionic strength by addition of 500 mM NaCl. **e,** Control spectra of CrataBL at 500 mM NaCl.

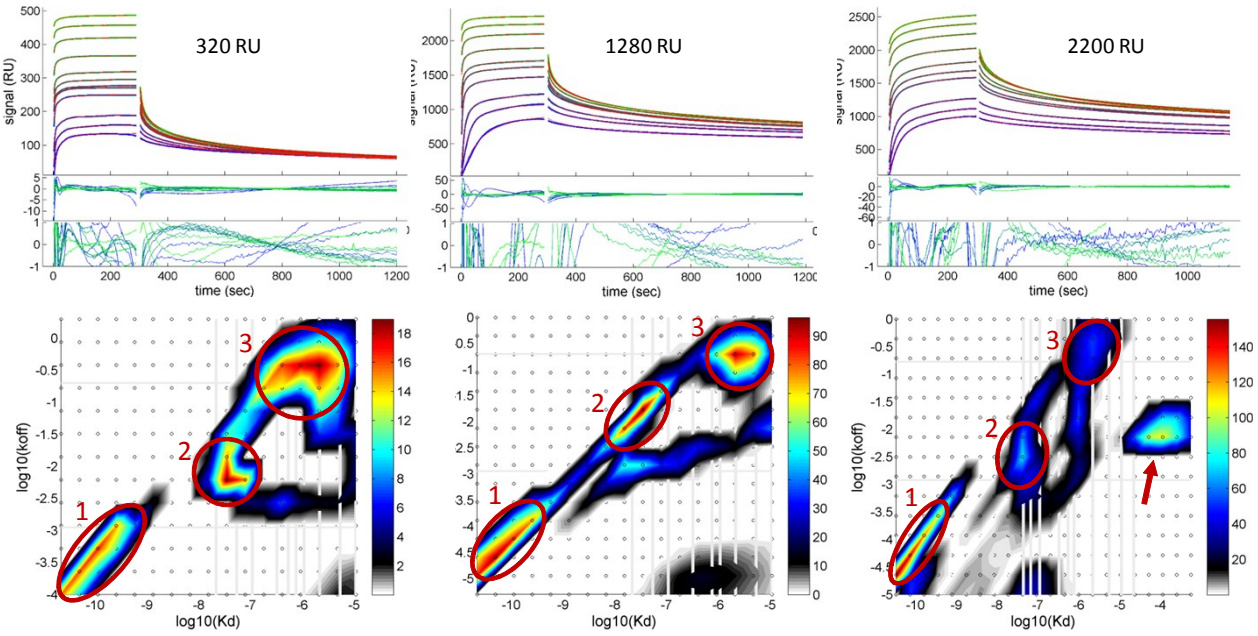

Figure S6. Characterization of AuMBA-CrataBL interactions by surface plasmon resonance. CrataBL was immobilized at surface densities of 320, 1280 and 2200 RU. AuMBA was injected in the flow to interact with all three surfaces simultaneously. Top panels: shown are the experimental traces (green and blue lines), best-fit curves (red lines), and fitting residuals. Bottom panels: calculated affinity and rate constant distributions from corresponding traces shown on top. Circled regions indicate the major peaks in the distributions. Integrated values are shown in Table S1. An extra low-affinity peak appears in the distribution calculated from the highest immobilization density (arrow).

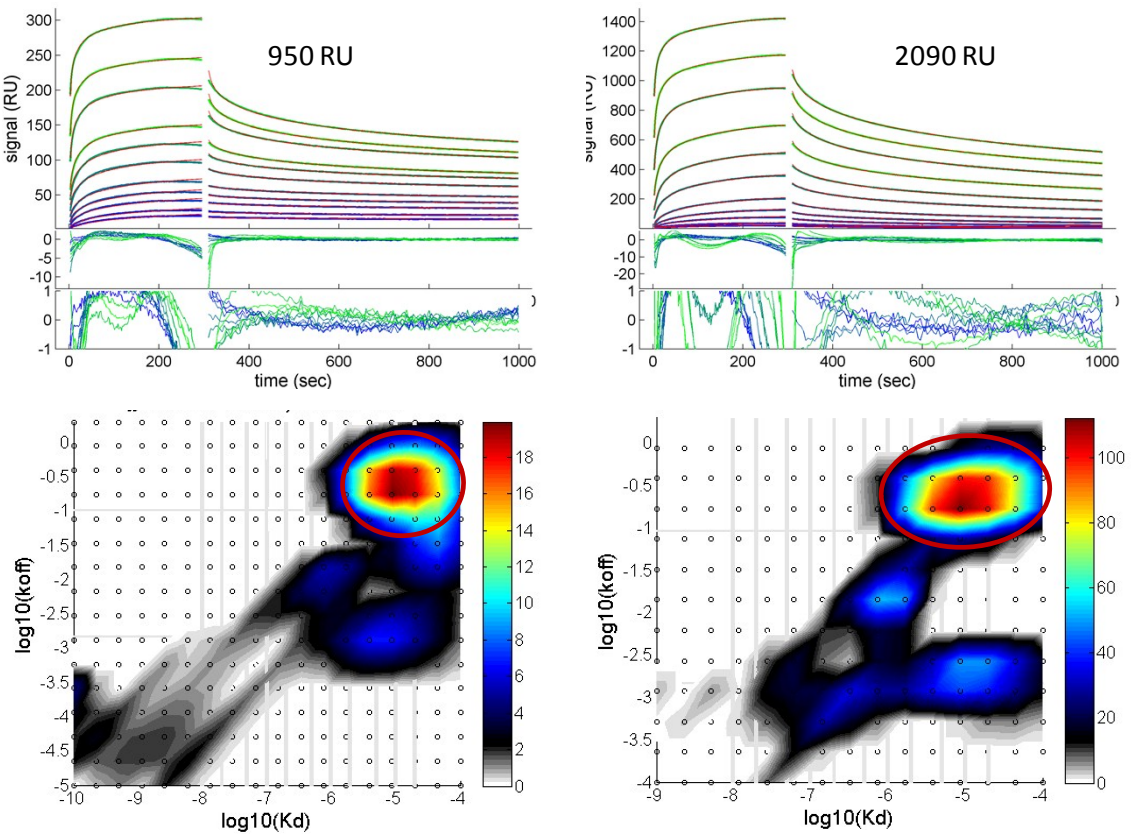

Figure S7. Characterization of AuGSH-CrataBL interactions by surface plasmon resonance. CrataBL was immobilized at surface densities of 950 and 2090 RU. AuGSH was injected in the flow to interact with both surfaces simultaneously. Top panels: shown are the experimental traces (green and blue lines), best-fit curves (red lines), and fitting residuals. Bottom panels: calculated affinity and rate constant distributions from corresponding traces shown on top. Circled regions indicate the major peaks in the distributions. Integrated values are shown in Table S2.

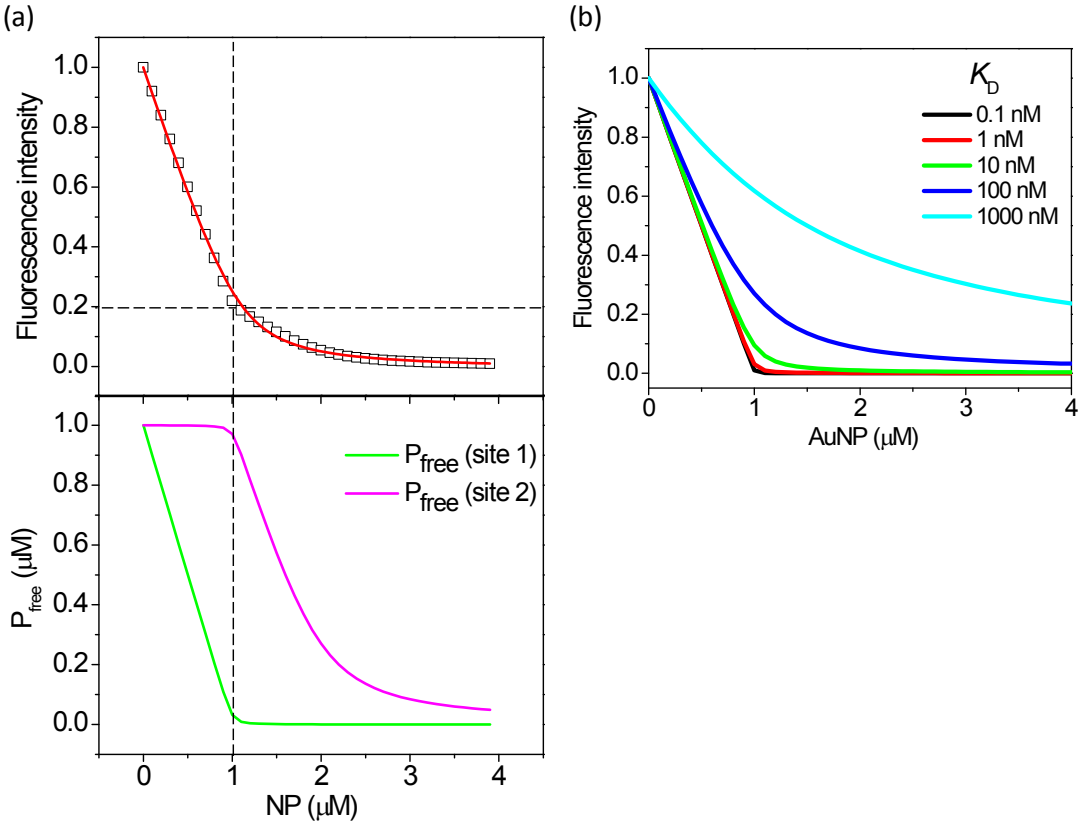

Figure S8. Simulation of steady-state fluorescence quenching. a, Simulated fluorescence quench data assuming binding of two NPs to a single protein. The individual K_{Ds} were set to 0.1 and 100 nM. Additional parameters included: F_0 = 1, n = 1 and $[P]_t$ = 1 μM. Under these conditions the NPs saturate the high-affinity protein site (site 1) before the second site (site 2) is occupied (see lower panel for calculated $[P]_{free}$ as a function of the total $[NP]$). It is also assumed that NP binding to the high-affinity protein site produces an 80% drop in fluorescence, and that binding of a second NP to the lower-affinity site quenches the remaining fluorescence. The second binding event creates a curvature in the quenching curve starting at the level of the remaining protein fluorescence (upper panel). Calculation of K_D with the quadratic equation (fitted curve shown in red) yields 60 nM, and the high-affinity site remains "invisible". **b**, Simulated NP-protein quenching data for different values of the affinity constant K_D. Additional parameters: F_0 = 1, n = 1, F_s = 0, $[P]_t$ = 1 μM. When the K_D falls below ~ 10 nM the traces lose their curvature and become indistinguishable from each other (the stoichiometric binding condition).

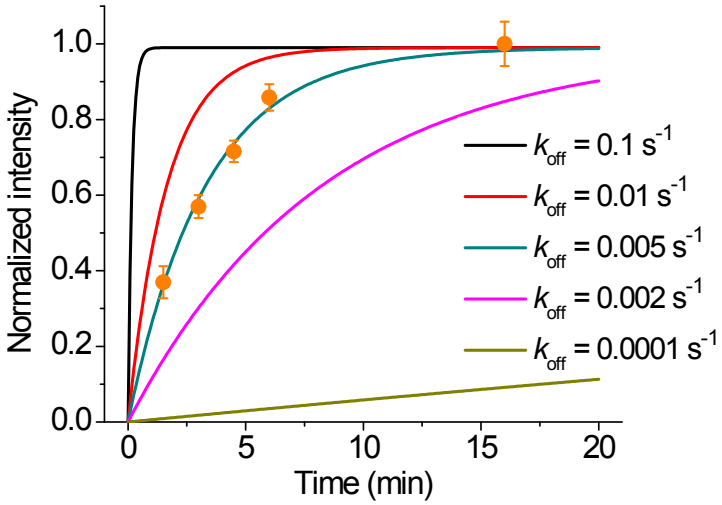

Figure S9. Estimation of k_{off} for AuMBA-CrataBL. The dissociation of CrataBL from AuMBA particles immobilized onto micrometer magnetic beads was followed as a function of time by measuring the intrinsic fluorescence of dissociated CrataBL in a fluorimeter. Normalized fluorescence values of dissociated CrataBL are shown as orange circles. Extending the readout time to over 3h does not yield a significant increase in fluorescence (< 10%). Solid lines show calculated values for comparison. The experimental results are consistent with a k_{off} roughly around 0.5×10^{-2} s^{-1}. Comparison with simulations clearly rules out the possibility of a k_{off} in the 10^{-4} s^{-1} range.

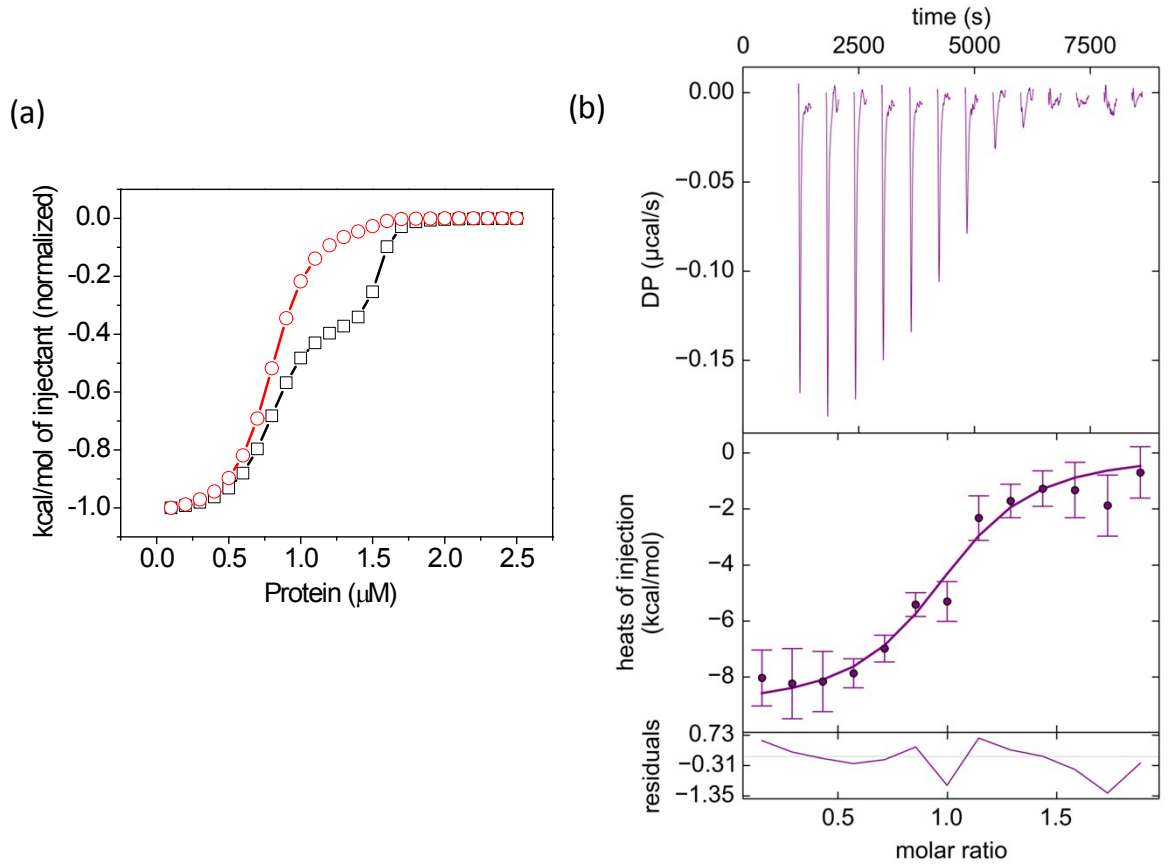

Figure S10. Simulated and experimental ITC data for AuMBA-CrataBL interactions. a, Simulated ITC isotherm assuming the presence of two binding sites on CrataBL (with K_{Ds} of 0.1 and 100 nM) and no binding cooperativity. Black squares: assuming NP binding to high-affinity site generates twice as much exothermic heat as binding to lower-affinity site. Here the individual binding events can be detected from a single ITC isotherm. Red circles: assuming NP binding to both protein sites generates equal heats. Here the individual binding events cannot be detected. **b**, Experimental ITC data and fitted curve for AuMBA-CrataBL assuming an independent binding-site model. Calculated K_D = 230 nM.

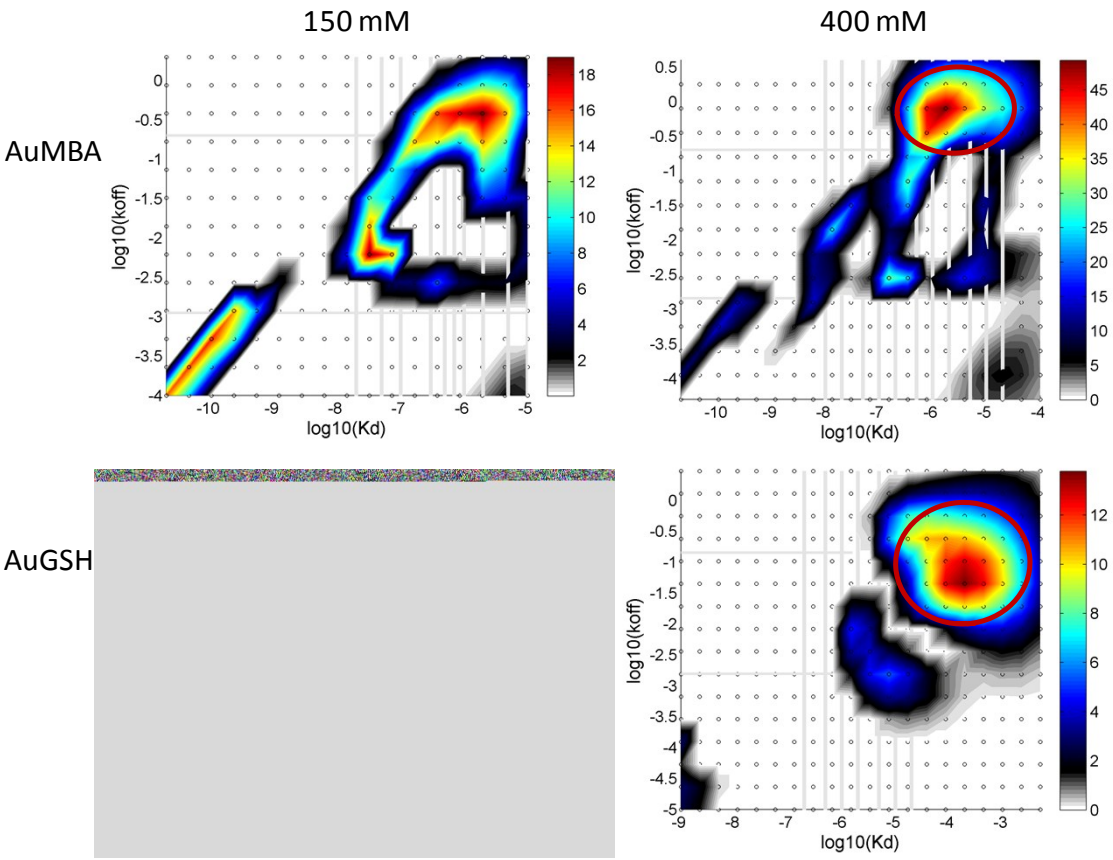

	AuMBA	AuGSH
K_D (M)	(2.9 ± 0.5)x10^{-6}	(2.2 ± 0.1)x10^{-4}
k_{on} ($M^{-1}s^{-1}$)	(2.2 ± 0.7)x10^{5}	(8.1 ± 5.0)x10^{2}
k_{off} (s^{-1})	(6.4 ± 3.2)x10^{-1}	(1.8 ± 1.2)x10^{-1}

Figure S11. Effect of NaCl concentration on the affinity and kinetics for AuMBA- and AuGSH-CrataBL interactions. Phosphate buffer supplemented with either 150 or 400 mM NaCl was used as running buffer. Circled regions indicate the major peaks in the distributions for 400 mM. Table shows the average affinity and kinetic constants from the experiments performed at 400 mM NaCl. These values can be compared to those obtained at 150 mM NaCl (Table 1).

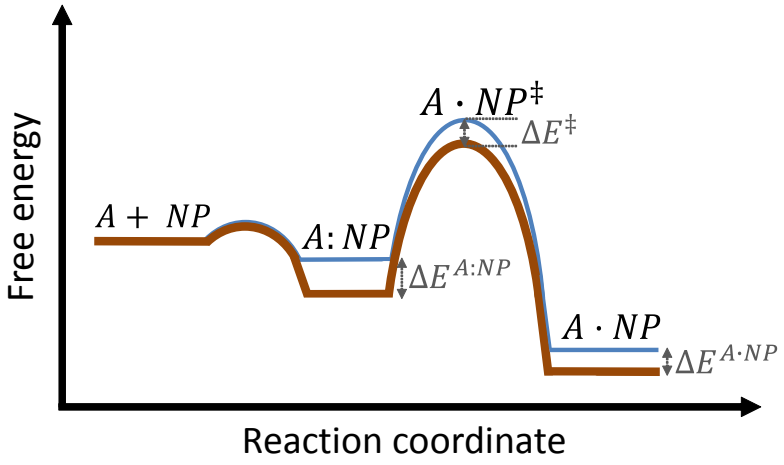

Figure S12. Free energy of interaction per the adopted reaction model (Eq. 2, main text). Four main states are represented: the unbound protein and NPs ($A + NP$), the encounter complex ($A{:}NP$), the transition state ($A \cdot NP^{\ddagger}$), and the bound complex ($A \cdot NP$). The height of the transition state barrier defines the association mode: diffusion- vs. reaction limited. Represented in blue is the proposed free energy diagram at a higher ionic strength. In comparing the two diagrams, it has been assumed that: First, the energy levels of the transition state ($E^{\ddagger}$) and final complex ($E^{A \cdot NP}$) are destabilized to a similar extent under higher ionic strengths. Thus, $\Delta E^{\ddagger} \sim \Delta E^{A \cdot NP} > 0$. A similar assumption is often invoked to explain the weak influence of ionic strength on k_{off} in the interactions between proteins [s6]; Second, the encounter complex is more strongly destabilized at higher ionic strengths relative to the transition and final states, since the encounter complex is more accessible to water and ions [s7]. Thus, $\Delta E^{A:NP} > \Delta E^{\ddagger} \sim \Delta E^{A \cdot NP} > 0$. (Note that in the main text $\Delta E^{A:NP} \sim \Delta E^{\ddagger} \sim \Delta E^{A \cdot NP}$ was assumed for simplicity); Third, the energy barrier to reach the encounter complex remains unaltered with ionic strength, since the association of CrataBL to the NPs is not strongly stereospecific. These considerations enable to tentatively predict how the individual kinetic rate constants (k_1, k_{-1}, k_2, k_{-2}) might change as the ionic strength is increased: (i) $k_{-2} \sim$ constant; (ii) $k_1 \sim$ constant. (This observation regarding k_1 contrasts with that for geometrically restricted interfaces in protein-protein complexes, where k_1 may depend strongly on the magnitude of long-range electrostatic forces [s8]); (iii) k_{-1} increases. (iv) k_2 increases; (v) k_{-1} increases more relative to k_2. The above predicted changes in the rate constants can be substituted in the k_{on} and k_{off} expressions for AuMBA- and AuGSH-CrataBL (Eqs. 3 and 4 in the main text): for AuMBA, k_{on} is predicted to remain constant and k_{off} to increase with ionic strength; for AuGSH, k_{on} is predicted to decrease and k_{off} to remain constant.